Progress In Electromagnetics Research C, Vol. 122, 253–266, 2022

Design of Filter Integrated SPDT Switch Using Capacitor Loaded Ring Resonator with High Isolation

Zayed A. Nasser, Noor A. Shairi*, Zahriladha Zakaria, Siti N. Zabri, Abdullah M. Zobilah, and Husam Alwareth

Abstract—A reconfigurable filter integrated single-pole double-throw (SPDT) switch (FIS) based on capacitor loaded ring resonators is presented in this paper. The design incorporates two PIN diodes between two symmetric square ring resonators. The ring resonators can be switched between allstop and bandpass responses, by adjusting the state of the PIN diodes, allowing the corresponding signal path to be in OFF-state with high isolation or ON-state with bandpass filter response. For demonstration, filtering switch was fabricated and measured for 2.4 GHz applications. The measurement results featured an ON-state low insertion loss of −2.1 dB and port-to-port isolation of −52 dB at the band of interest, and good consistency is achieved between simulated and measured results.

1. INTRODUCTION

Integrating multiple RF components into one single module is an effective approach to minimize circuit size, mismatching loss, and power consumption. Various multifunctional microwave circuits have been successfully demonstrated, including antenna integrated with RF switch [1, 2], integrated filter antenna [3–5], and even power amplifier integrated with antenna [6].

Bandpass filter (BPF) integrated single-pole double-throw (SPDT) switch (FIS), as depicted in Figure 1, is another integrated/multifunction device. Many efforts, i.e., reused switchable L-shaped resonator [7], dual-mode microstrip-cavity structures [8], suspended-controllable resonators [9], standing-wave-filtering structures [10], capacitively-coupled LC resonators with loaded PIN diodes [11], switchable T-shape resonators [12], distributed coupling quarter-wavelength resonator with loaded PIN diode [13], in-house developed 3D-TSV-MEMS [14], and fractal stub-loaded resonator (F-SLR) [15], have been developed to integrate filters and SPDT switches. Nevertheless, the aforementioned filtering-SPDT switch works suffered from high insertion loss (IL) [11–14], low ports isolation [8–15], or low-frequency selectivity [7–9].

The isolation of the RF filtering switch is also a major issue to avoid leakage currents. Nowadays, intensive research is going on to develop high isolation of RF filtering integrated switches. In [16], a common shorted stepped-impedance resonator technique is used and produces isolation of −58 dB. In [17], two distributed coupling identical tri-mode resonator (TMR) pairs loaded with opposite polarity PIN diodes are proposed and achieve high isolation of $-50/-43$ dB at the frequency band of 0.9 GHz/1.8 GHz. The authors develope a new switch using substrate integrated suspended line (SISL) technology in [9] and report that a multilayer produces better isolation below −40 dB at 1 GHz. In [18], a parallel switched fractal common feeding line switch to provide four identical coupling paths

Received 18 March 2022, Accepted 3 August 2022, Scheduled 17 August 2022

* Corresponding author: Noor Azwan Shairi (noorazwan@utem.edu.my).

The authors are with the Microwave Research Group (MRG), Centre for Telecommunication Research & Innovation (CeTRI), Fakulti Kejuruteraan Elektronik dan Kejuruteraan Komputer (FKEKK), Universiti Teknikal Malaysia Melaka (UTeM), Hang Tuah Jaya, Durian Tunggal, Melaka 76100, Malaysia.

is proposed and produces the isolation of −45.7 dB at 0.99 GHz. A type of bandpass filter (BPF)-integrated SPDT switch using frequency-selective star-junction matching circuit technique is proposed in [19]. The isolation achieved is −47.8 dB which operates around the 1 GHz frequency. Although these reported filter-integrated switches can provide high isolation, there is a trade-off in terms of the number of switching elements (PIN diode) required to perform the function, resulting in an increase of bias circuit complexity.

In this paper, a technique to design a bandpass filter integrated SPDT switch by using a capacitor loaded ring resonator is proposed. The design and analysis of a ring filtering switch are described in this paper. The design belongs to SPDT switch category, which is utilized in Time Division Duplex (TDD) communication for simultaneous transmitting and receiving operations. A capacitor-loaded square ring resonator is the basis of the proposed design. To select between allstop and bandpass responses, PIN diodes are employed as switching components. The suggested design has been validated at 2.4 GHz through insertion loss, return loss, and isolation performance. The proposed integrated filtering switch provided several benefits, including removing out-of-band signals, good filtering performance in the ON-state, and high isolations in the OFF-state.

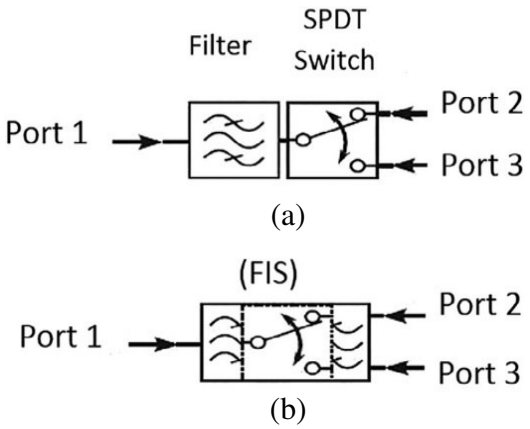

Figure 1. Diagram of (a) bandpass filter and SPDT switch, (b) cascaded BPF and SPDT switch integrated filter SPDT switch [20].

2. BANDPASS FILTER DESIGN

2.1. Bandpass Filter Configuration

The bandpass filter's development begins with implementing a square shape ring resonator, followed by introducing a microstrip line coupled with the square resonator with a space $a = 0.5$ mm. An L-shaped slot was cut in the resonator feed line to suppress higher undesirable frequencies.

As illustrated in Figure 2, the ring resonator unit is parallel-coupled to the microstrip transmission line. The entire length of the ring resonator is full wavelength at the resonance frequency, λ. The wavelength is $\lambda/4$ for each l_1 length, forming a square-shaped ring resonator.

The resonator was designed based on microstrip equations (1) to (5). The list of equations involved is shown below [21].

$$\frac{w}{d} = \frac{8e^A}{e^{2A} - 2} \tag{1}$$

where w is the conductor width, and d is the dielectric substrate thickness.

$$A = \frac{Z_o}{60}\sqrt{\frac{\varepsilon_r + 1}{2}} + \frac{\varepsilon_r - 1}{\varepsilon_r + 1}\left(0.23 + \frac{0.11}{\varepsilon_r}\right) \tag{2}$$

where ε_r is the relative permittivity.

$$\varepsilon_{eff} = \left(\frac{\varepsilon_r + 1}{2} + \frac{\varepsilon_r - 1}{2}\right) \cdot \frac{1}{\sqrt{1 + 12\left(\frac{d}{w}\right)}} \tag{3}$$

$$l = \frac{\frac{1}{4} \times 2\pi}{\beta} \tag{4}$$

where l is the line length.

$$\beta = k\sqrt{\varepsilon_{eff}} \tag{5}$$

where k is the propagation constant.

The initial length (l_1) and width (w) were 19.3 mm and 2.8 mm, respectively. However, it created a resonance at 2.5 GHz, and some tuning was done for resonant frequency shifting. Thus, the proposed structure in Figure 2 was simulated in CST software on an FR4 substrate with a thickness of 1.6 mm and permittivity of 4.7. The optimized parameter values in (mm) are $l_1 = 19.6$, $L_m = 2.5$, $S = 21$, $g = 0.5$, $W = 2.8$, $W_2 = 2.48$, $a = 0.5$, $e = 11.5$. The proposed filter unit is excited by Port 1 and Port 2 feed lines of 50 ohms.

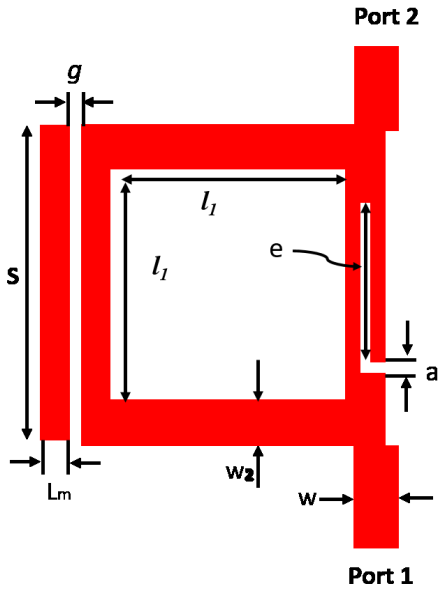

Figure 2. Proposed bandpass filter.

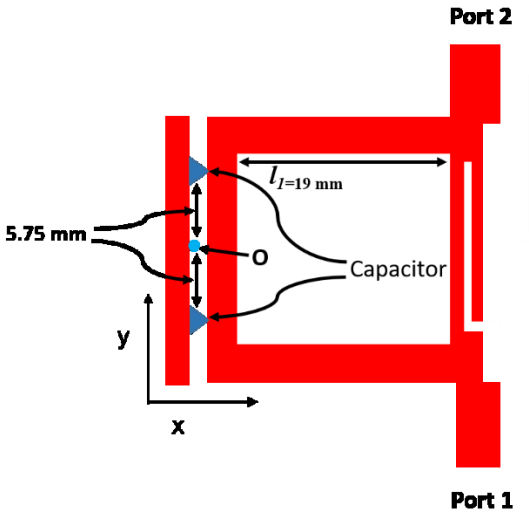

Figure 3. Proposed filter loading with two capacitors.

2.2. Bandpass Design Evaluation

The resonant frequency is known to be inversely proportional to inductance and capacitance. The resonant frequencies can be moved to lower frequencies if the capacitance (C) of the resonator is increased [22]. The lumped capacitor enhances the effective capacitance and reduces the filter size, resulting in improved filter performance by enhancing the resonator's stored energy. Therefore, two 1 pF lumped capacitors were installed within the space between the square ring resonator and microstrip transmission line. Figure 3 depicts the conventional schematic view of the bandpass filter with two loaded lumped capacitors loaded within the space between the ring resonator and microstrip line. The capacitors were placed at a distance of 5.75 mm from the microstrip line center (denoted as point O in Figure 3) along the y-axis. The proposed bandpass filter indicated in Figure 4 was simply simulated and modeled using CST software.

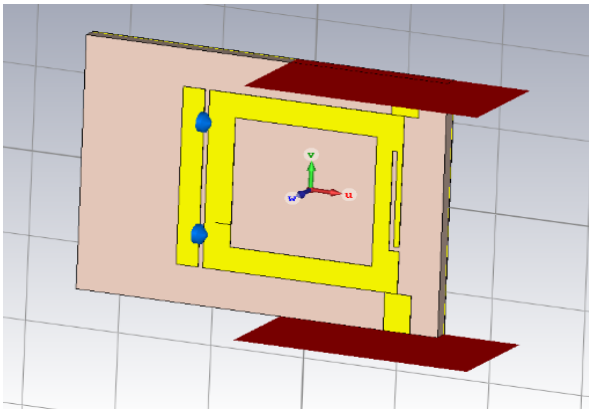

Figure 4. 3D model of the ring resonator structure in CST software.

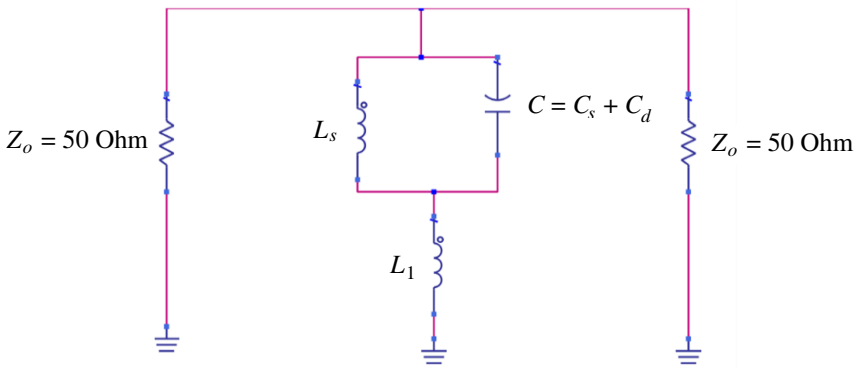

Figure 5. Equivalent circuit of the proposed BPF at 2.4 GHz.

The bandpass filter shown in Figure 4 was modeled using a shunt series resonant branches equivalent circuit [23] as shown in Figure 5.

The inductance and capacitance of the BPF were evaluated using the following equations [24]:

$$C_d + C_s = \frac{\pi}{\omega_0 Z_o} \tag{6}$$

$$L_s = \frac{1}{\omega_0^2 C} \tag{7}$$

The inductance of the microstrip line was evaluated using the following equation [24]:

$$L_1 = \frac{1}{\omega_0} \times Z_o \times \sin\left(\frac{2\pi l}{\lambda_g}\right) \tag{8}$$

where ω_0, the resonance, is (tuned) angular frequency, and λ_g is the guided wavelength.

The input impedance extracted from the equivalent circuit was evaluated using the following equations [24]:

$$Z_{in} = \frac{j\left[\omega^2 L_s\left(C_s + C_d\right) - 1\right]}{\omega C_d\left(1 - \omega^2 L_s C_s\right)} \tag{9}$$

L_s and C_s are the shunt circuit of the design considered as a lossless resonator. Furthermore, the installed capacitor (C_d) is distinguished from the natural capacitance of the resonator denoted as C_s.

When $Z_{in} = 0$, the resonant frequency can be expressed as:

$$\omega_0 = \frac{1}{\sqrt{(L_s)(C_s + C_d)}} \tag{10}$$

The above equations show that the resonant frequencies move to lower frequencies if the resonator total capacitance value $C(C_s + C_d)$ is increased. This equation demonstrates that the greater the capacitance value is, the lower the operating frequency is.

A parametric study for loaded capacitors value (C_d) was done, and the ideal value was determined as indicated below to obtain optimum performance at 2.4 GHz while maintaining a compact filter circuit.

As shown in Figure 6, the filter operating frequency is operational to the loaded capacitance values (C_d). The bandpass filter has a central frequency of 3.7 GHz; however, the center frequency changes to lower values when a lumped capacitor C_d was applied. The resonant frequencies were reduced by 72 percent when two 1 pF capacitors were applied, implying that the addition of lumped capacitors leads to smaller sizes. Furthermore, when the lumped capacitors were increased, the operational bandwidth of the proposed filter decreases due to increases in the filter quality factor (Q) caused by a decrease in radiation loss. This finding is consistent with the expectation, because the quality factor is defined as:

$$Q = \omega_0 \frac{E_{sto}}{R_{loss}} = \omega_0 \left(C_s + C_d\right) R = \frac{\omega 0}{B} \tag{11}$$

where ω_0 is a resonance (tuned) angular frequency, E_{sto} the stored energy, R_{loss} the radiation loss, R the resistance of the resonator, and B the bandwidth.

The selected capacitors value can be used to adjust the BPF central frequency across various operating bands. For example, a 1 pF value was used for the capacitor to alter the resonance frequency from 3.5 GHz (WiMAX) band to the lower 2.4 GHz (WLAN) band.

Also, a downshift in operating frequency has resulted in the miniaturization of the overall resonator size. Based on Equations (9) and (10), the miniaturized bandpass filter is easily realized by applying the parallel two 1 pF lumped capacitors (C_d).

The simulated S-parameters ($|S_{11}|$ and $|S_{21}|$) results of the proposed bandpass filter are illustrated in Figure 7. The filter is operated at a center frequency of 2.4 GHz with 100 MHz bandwidth. The matched return loss was −25 dB, while the achieved insertion loss was −2 dB at the band of interest.

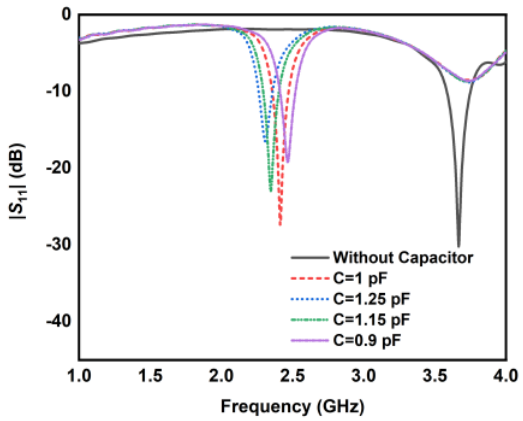

Figure 6. $|S_{11}|$ of the proposed filter with different values of lumped capacitor.

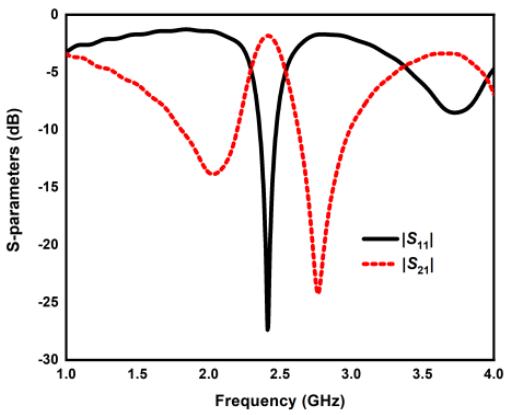

Figure 7. $|S_{11}|$ and $|S_{21}|$ simulated results of the BPF filter.

Figure 8 shows the prototype of the proposed bandpass filter. The layout total size of the filter structure is 26 mm × 26 mm.

The filter-designed simulation results using CST and measurement results using vector network Analyzer (N5242A) from Keysight Technologies are presented in Figure 9. The simulated and measured return losses were better than −25 dB at 2.4 GHz, while the measured insertion loss was around −2.1 dB at the band of interest. There is a good agreement between the two results; however, a slight shift in the center frequency from 2.4 GHz to 2.42 GHz is observed in the measured result, which is due to the permittivity variation of the FR-4.

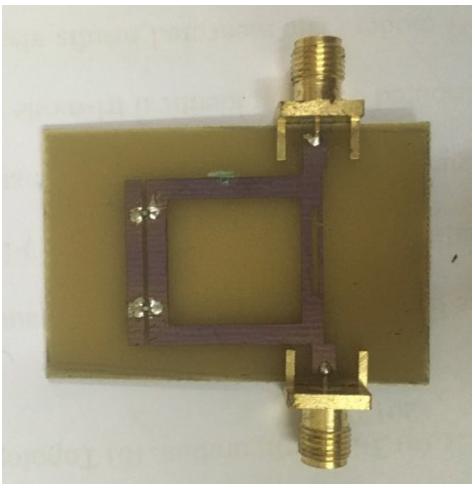

Figure 8. Prototype of the proposed filter.

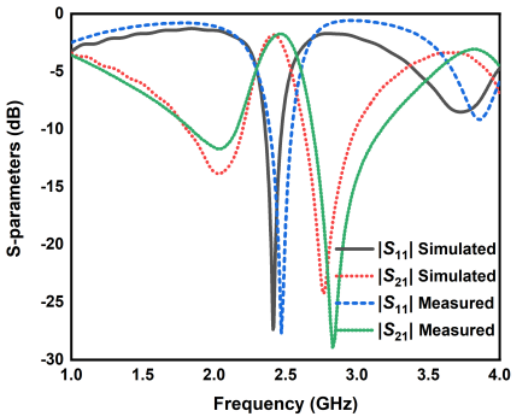

Figure 9. The simulated and measured $|S_{11}|$ and $|S_{21}|$ for the bandpass filter.

3. FILTER INTEGRATED SPDT SWITCH

The configuration of the proposed filter integrated SPDT switch design based on the square ring resonator, presented in Section 2, is shown in Figure 10.

At first, the square ring filter resonator is symmetrically mirrored to build a single-pole-double-throw switch (SPDT) having bandpass filtering function and reasonable isolation between transmitter and receiver. The filter ring resonator at the receiver side (Port 2) is a mirror image of the filter resonator at the transmitter side (Port 1) to minimize detuning of one side with respect to another as both arms operate at the same frequency band. Then, the filter integrated SPDT switch structure is extended to a three-port design by adding another microstrip transmission line section with a third port (Port 3) or known as the antenna port. Both switch transmission paths share this common microstrip transmission line at Port 3.

Generally, this filter integrated SPDT switch was designed to switch the RF signal between transmitter and receiver modes with a good bandpass filtering response. The series PIN diodes (D2 and

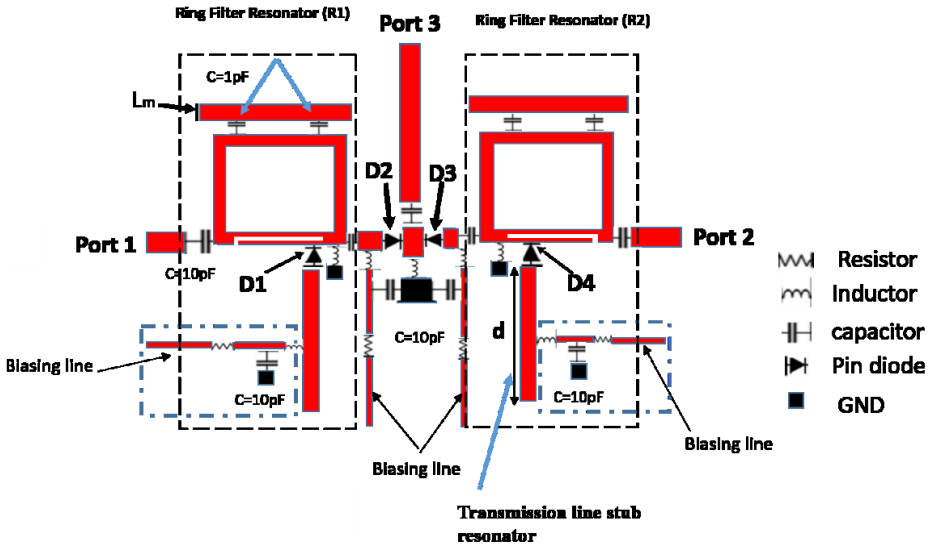

Figure 10. Proposed filter integrated SPDT switch simulated structure.

D3) were used for this purpose. Transmission line open stub resonator (d) was connected to the shunt PIN diodes (D1 and D4) to achieve additional isolation improvement. The addition of the transmission line stub resonator (d) provided additional current path flow, and hence further isolation was achieved.

3.1. Transmitter Mode

Filter integrated SPDT switch structure was designed to route the RF signal between transmitter mode (Tx) and receiver mode (Rx) while keeping a good filtering response simultaneously. Figure 11 represents the circuit operation of the proposed RF filtering switch in transmitter mode. When the RF input power is induced to the Tx port (Port 1), the ring filter R1 is activated, and the ring filter R2 is deactivated so that Port 2 is directly grounded through a 50 Ω resistor.

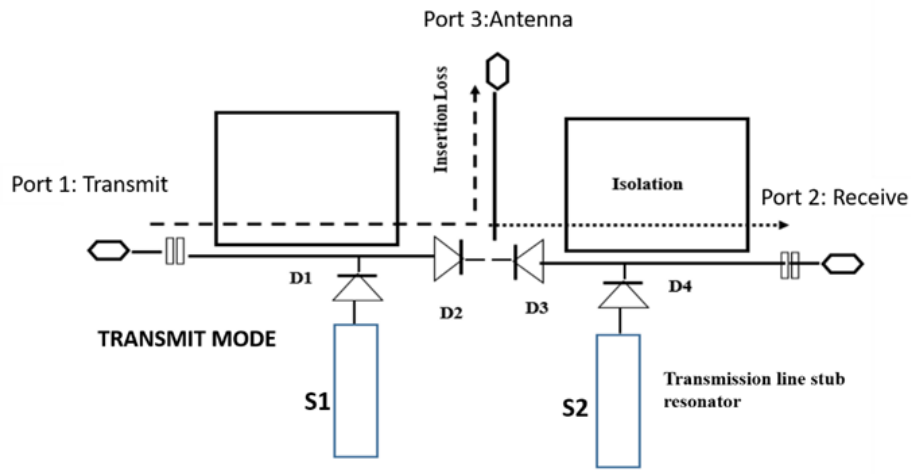

Figure 11. Circuit diagram of the proposed filtering switch (Transmitter mode).

In this state, the RF signal transmitted from Port 1 (Transmitter) to Port 3 (Antenna) is considered an insertion loss. The transmitter chain should produce very low RF signal leakage. The isolation between Port 2 (Receiver) and Port 1 (Transmitter) is attained from the deactivated state of the PIN diode (D3) in the receiver chain.

Additionally, the ON state of PIN diode D2 allows the RF signal to transmit to Port 3 (Antenna) easily. Obviously, in this operation, the isolation between transmitter and receiver results from the allstop behavior of ring filter R2 at the receiver (receiver) side. In addition, filtering of the transmitted signals results from the bandpass capability of the ring filter (R1) at the transmitter side. As a result, an all-pass response was produced by transmission line open stub resonator **S1**. On the contrary, a shunt PIN diode in the receiver (Rx) arm D4 is switched ON with voltage control of +5 V. As a result, the bandstop response is produced by transmission line open stub resonator **S2**.

3.2. Receiver Mode

As shown in Figure 12, during the receiver mode operation, RF signals flow from the antenna (Port 3) to the receiver (Port 2). When the RF input power is induced to the Rx port (Port 2), the ring filter R2 is activated, and the ring filter R1 is deactivated so that Port 1 is directly grounded through a 50 Ω resistor. During this state of operation, RF signals propagate from antenna to the receiver (Rx). In this mode, series PIN diode D3 is activated, whereas shunt PIN diode, in the receiver chain, D4 is deactivated with voltage control, 5 V.

The ring filter R2 acts as a bandpass filter during this condition, while the ring filter R1 acts as an allstop filter. Furthermore, the ON state of PIN diode D3 allows the RF signals to transmit through Port 2 freely.

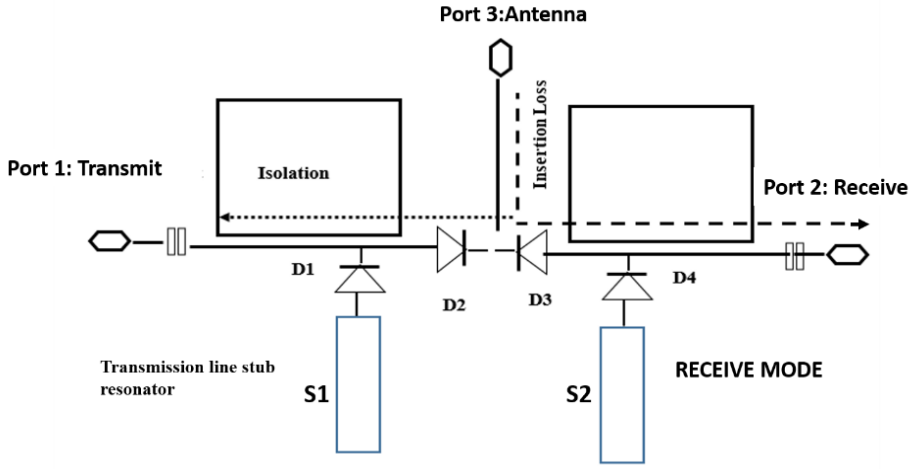

Figure 12. Circuit diagram of the proposed filtering switch (Receiver mode).

Obviously, in this operation, the isolation between the two arms results from the allstop response of R1 at the transmitter side. In addition, filtering of the transmitted signals results from the bandpass capability of ring filter R2 (at the receiver side). In this scenario, a shunt PIN diode in the transmitter (Tx) arm D1 is switched ON with voltage control of +5 V. As a result, a bandstop response was produced by transmission line open stub resonator **S1**. On the contrary, a shunt PIN diode in the receiver (Rx) arm D4 is switched OFF with voltage control of −5 V. As a result, an all-pass response was produced by transmission line open stub resonator **S2**.

Figure 13 shows the current distribution of the proposed filter integrated SPDT switch at 2.4 GHz. As observed in Figure 13(a), when the structure works at transmitter mode (Port 1 is excited), a strong current flowed along the filter resonator 1. The current on the receiver side (Filter Resonator 2) is considerably suppressed. On the contrary, when the structure is in receiver mode (Port 2 is activated), the current mostly concentrates on the filter resonator 2. The current on the channel of the transmitter side (Filter Resonator 1) is very weak, as can be observed in Figure 13(b). This current distribution indicated that good filtering performance and extremely excellent port-to-port isolation was obtained.

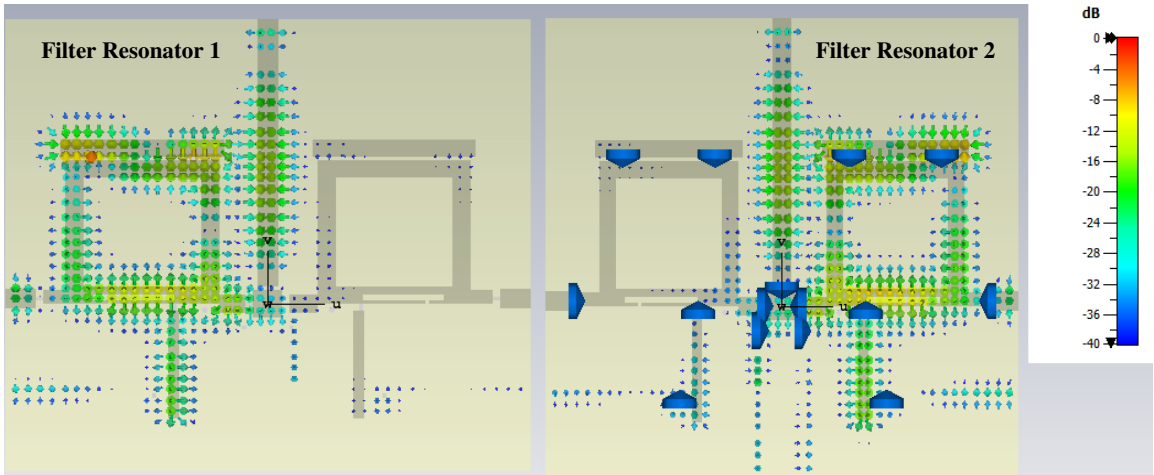

(a) (b)

Figure 13. Current distribution of the proposed filter integrated SPDT switch at (a) transmitter mode and (b) receiver mode.

4. SIMULATION AND MEASUREMENT RESULTS OF FILTER INTEGRATED SWITCH (FIS)

To testify the feasibility of the theoretical and simulated analysis carried out in Section 3, the proposed filtering switch was fabricated as shown in Figure 14. The design performance was validated by comparing simulated results with their measured counterparts. The FR4 material with a relative permittivity (ε_r) of 4.7 and a thickness of 1.6 mm was used to fabricate the proposed filtering switch design. The low-cost PIN diodes with part numbers of BAP64-02 from NXP were used to switch between the two transmission paths (Port 1 and Port 2). The states of the PIN diodes were controlled by the bias circuits with a voltage of 5 V through a capacitor and inductor with values of 10 pF and 10 nH, respectively. The value of resistors at the input of biasing circuit was set to 47 Ω to limit the biasing current of PIN diodes.

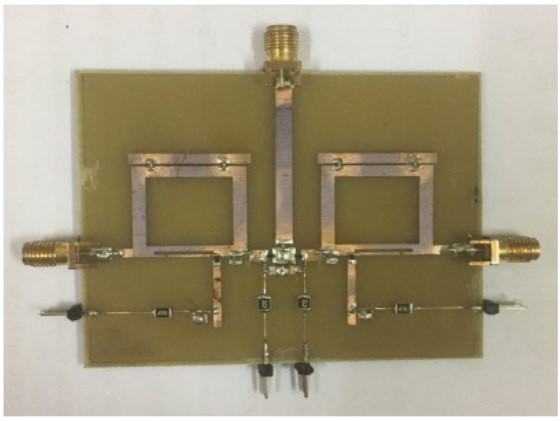

Figure 14. Prototype of the suggested filter integrated SPDT switch.

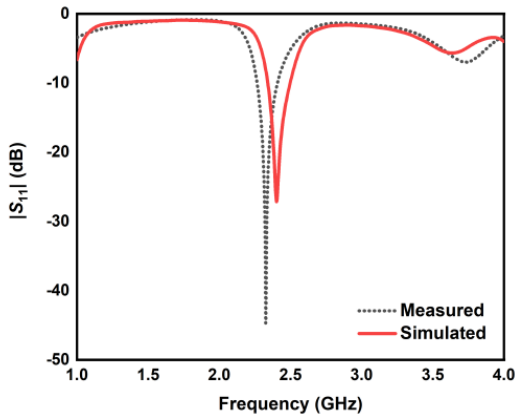

Figure 15. Simulation and measurement return loss of the filter integrated SPDT switch at Tx mode.

The fabricated module of the proposed filter integrated SPDT switch design was based on a square ring filter resonator. The total size of the proposed filter integrated switch is 66 mm × 70 mm. The filter-integrated SPDT switch was designed for wireless applications in 2.4 GHz bands and was built using the microstrip model in CST software.

Because of the completely symmetric bandpass filter unit on both sides of the structure, the signals at the two output ports are exactly the same. Thus, in the following sections, only the transmitter mode (Tx) operation is investigated, by which Port 1 is switched ON and Port 2 switched OFF.

Figure 15 displays the simulated and measured results of the proposed filter integrated SPDT switch based on symmetric square ring filter resonators. When D2 and D4 PIN diodes are in ON status and D1 and D3 in OFF status, the circuit is in Tx mode, whereby Port 1 is ON-state, and Port 2 is blocked. Similarly, it acts as Rx mode when D2 and D4 PIN diodes are in OFF status and D1 and D3 in ON state. In both cases, the proposed filter integrated SPDT switch operates at 2.4 GHz. As can be observed from Figure 15, the return loss of the ON-state Port 1 ($|S_{11}|$) was above −25 dB at 2.4 GHz, featuring efficient bandpass responses and good input port matching at the Tx port. The simulated return loss was less than −25 dB at 2.4 GHz, while the measured return loss was less than −40 dB.

In Figure 16, the simulation and measurement results for the isolation between Tx and Rx are compared and found in good agreement. At 2.4 GHz resonant frequency, more than −50 dB isolation was achieved in both simulation and measurement results. By observing the circuit performances at the resonant frequencies, the simulated isolation, $|S_{21}|$, was −55 dB while the measured isolation was −51 dB. It was found that the isolation is always higher than −25 dB and −27 dB in simulation and measurement, respectively, within the overall frequency range from 1.1 to 4 GHz. Further improvement in the port-to-port isolation was obtained by cascading a single shunt PIN diode with transmission line

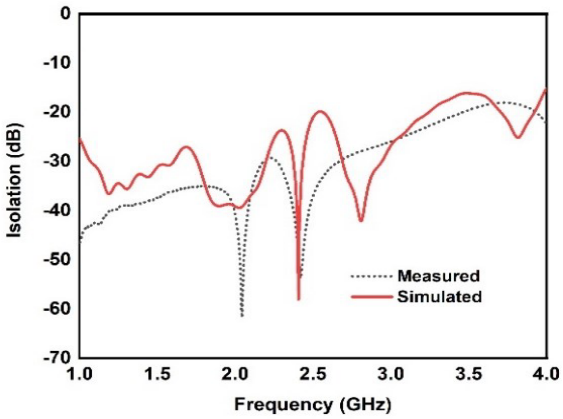

Figure 16. Simulated and measured isolation of the proposed filter integrated SPDT switch at Tx mode.

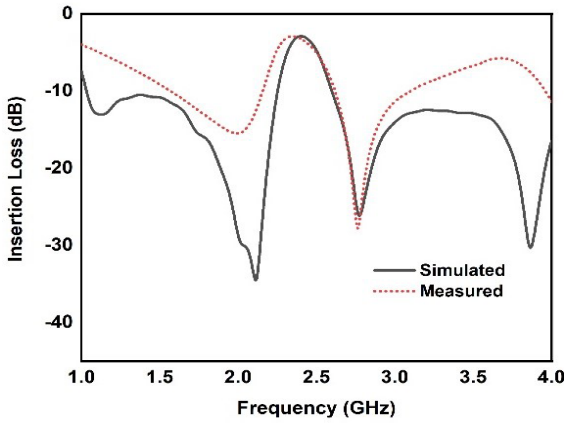

Figure 17. Simulated and measured insertion loss of the proposed filter integrated SPDT switch at Tx mode.

stub resonator (d) at each arm of the proposed design.

Figure 17 further illustrates that the proposed filter integrated SPDT switch has a low insertion loss at Port 3. The obtained insertion loss was −2.1 dB at a resonant frequency of 2.4 GHz with a 0.1 GHz bandwidth. As can be seen in Figure 17, the simulation result for insertion loss was −2.1 dB, while the measurement value for insertion loss was −2.17 dB. However, there is a minor discrepancy between measurement and simulation results which is attributable to parasitic capacitance and inductance of PIN diode, substrate tolerance, and solder wire resistance [25]. According to the equations from [21–26], it could be concluded that theoretically, zero insertion loss, $|S_{13}|$, can be obtained if single series connected PIN diode (in ON state) is cascaded with the ring resonator. However, in the implemented design, the insertion loss is slightly different from zero. It can be rationally assumed that the total obtained insertion loss is cumulative of the series connected PIN diode loss and the ring filter resonator loss.

Table 1. The summarization of operating cases of the filter integrated SPDT switch.

	Receiver Mode	Transmitter Mode
Voltage bias 2 and 4	-5 V	+5 V
Voltage bias 1 and 3	+5 V	-5 V
PIN diodes (D2 and D4)	OFF states	ON states
PIN diodes (D1 and D3)	ON states	OFF states
Ring Filter (R1)	Allstop characteristics	Bandpass characteristics
Ring Filter (R2)	Bandpass characteristics	Allstop characteristics
	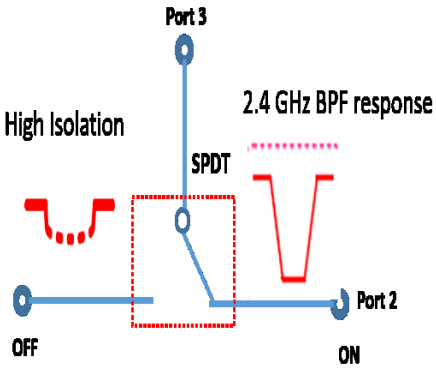	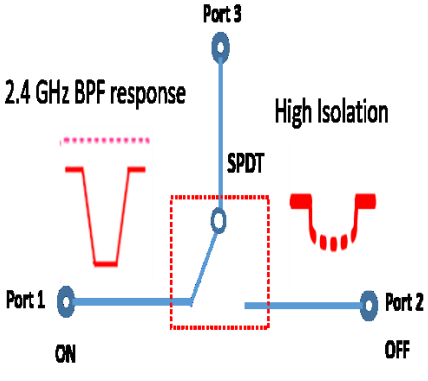

The results demonstrate that the proposed filtering switch has two operational modes, as clarified in Table 1.

5. PARAMETRIC STUDY

To obtain the best performance at 2.4 GHz while maintaining a small filter integrated SPDT switch size, a parametric analysis for the proposed design critical parameters was done, and the ideal values are determined as will be indicated below. The study of the essential dimensions (d, Lm) through filter integrated SPDT switch return loss and isolation performance is presented in the following discussion.

Figure 18(a) depicts the return loss of the proposed design with various transmission line stub lengths (d). It is obvious that there is a negligible shift in the resonant frequency for all length values. In addition, no significant change was observed in the return loss of the proposed design. To compromise the matched return loss response and high isolation, the parameter value of $d = 15.7$ mm was chosen for the proposed design.

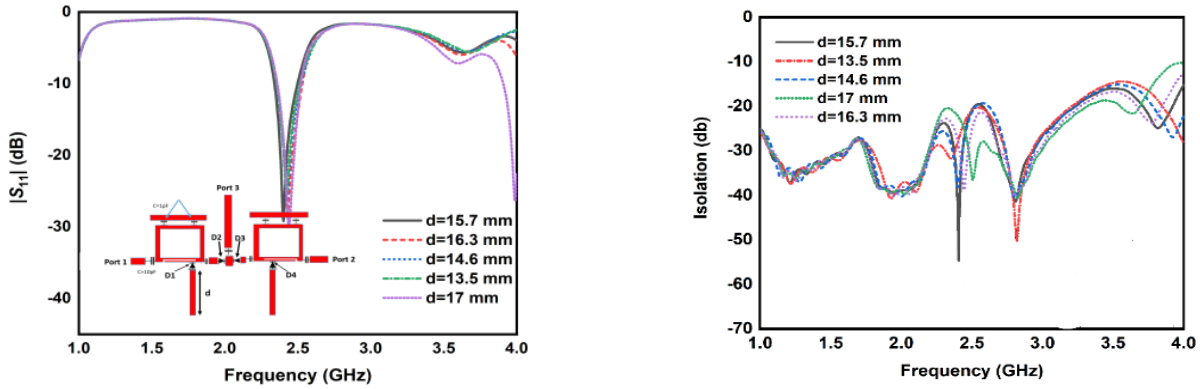

(a) (b)

Figure 18. Simulated filtering switch performance with different d: (a) $|S_{11}|$, (b) isolation.

Figure 18(b) compares the isolation performance of filter integrated SPDT switch with altering the length of transmission line stub 'd'. As observed, the isolation ($|S_{21}|$) of the filtering switch (FIS) achieved higher than -50 dB at 2.4 GHz operating frequency. Meanwhile, the isolation performance was better than -25 dB within a frequency range from 1 to 4 GHz. It can be observed that the best performance was achieved at $d = 15.7$ mm.

Figure 19 displays the bandpass filter's simulated $|S_{11}|$ and isolation with different microstrip line widths 'Lm'. The dimensions of Lm were varied from 2.5 mm to 0.6 mm. As observed, the operating frequency was shifted to lower values when transmission line width was decreased. It was observed that the resonant frequency was shifted to the center frequency of the ring resonator at 2.4 GHz by increasing m. In Figure 19(a), the return loss ($|S_{11}|$) shows a matched return loss response at 2.4 GHz when $Lm = 2.5$ mm, but by decreasing Lm to lower than 2.5 mm, it lowered the $|S_{11}|$ response, thus a trade-off between high isolation and matched $|S_{11}|$ was found when the optimal microstrip line width, Lm, was selected in the ring resonator design. This was because of the decrease in coupling spacing, concurrently with the decrease of Lm, thus strengthening the ring and microstrip line couplings.

Filtering switch isolation performances with changing the microstrip line width (Lm) are compared as presented in Figure 19(b). As observed, the isolation performance of the filter integrated SPDT switch (FIS) reached greater than -40 dB at 2.4 GHz resonant frequency. Meanwhile, the isolation performance was better than -25 dB within a frequency range from 1 to 4 GHz. It can be observed that the best performance was achieved at $Lm = 2.5$ mm.

A comparison between the proposed reconfigurable filter integrated SPDT switch possesses dual-functions (switching and filtering) simultaneously, and the reference filtering switch is summarized in Table 2. However, most of the reported designs in this literature produced high insertion loss and low

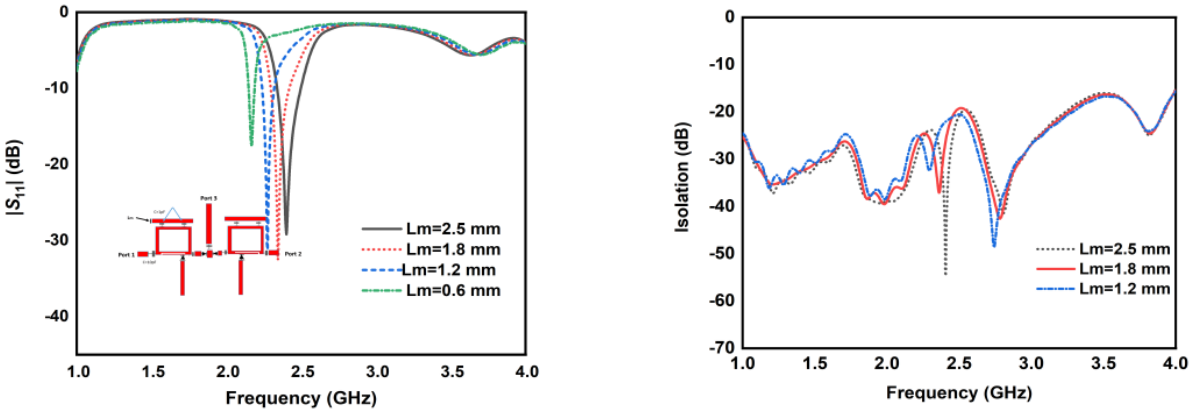

(a) (b)

Figure 19. Simulated filtering switch performance with different Lm: (a) $|S_{11}|$, (b) isolation.

Table 2. Comparison of recently published filtering switches with the proposed design.

References	Filter Topology	Frequency (GHz)	IL (dB)	Iso (dB)	PIN diodes per channel
[27]	BPF-SPDT-LC resonator	1	−2.7	−42	3
[28]	BPF-SPDT-Quasi-Lumped-Element	0.612	−2.8	−41.4	2
[19]	BPF-SPDT-Switched Magnetic Coupling	0.9	−1.52	−42	3
[17]	BPF-SPDT tri-mode resonator	0.99	−1.87	−50	4
[16]	BPF-SPDT-Stepped-Impedance Resonator	1	−1.99	−58	6
[12]	T-shape resonator	2.45	−4	−30.6	3
[18]	BPF-SPDT-Switched Fractal Common Feeding Line	0.99	−1.76	−45	3
This work	**Square Ring Resonator**	**2.4**	**-2.1**	**-52**	**2**

isolation. As can be shown, the filter integrated SPDT switch introduced in this study has comparable and satisfactory performances in terms of insertion loss and port-to-port isolation. Furthermore, the proposed design utilized a lower number of PIN diodes per channel to obtain the required isolation performance.

6. CONCLUSION

In this paper, a dual-function filter integrated SPDT switch based on a capacitor loaded ring resonator has been designed, fabricated, and measured for 2.4 GHz wireless applications. Square ring bandpass filter theory was studied and then implemented in the construction of a filter integrated SPDT switch. The proposed reconfigurable filtering switch can be switched between allstop and bandpass filter operations. The proposed switchable filter structure was successfully designed using CST software. More than −50 dB isolations, higher than −10 dB return loss, and low insertion loss were obtained in the realized performance, with good consistency between the simulated and measured results. These attractive features make the proposed filtering switch useful for many system applications such as time division multiplexing, multibeamforming array circuit, MIMO system, and other applications operating in 2.4 GHz band.

ACKNOWLEDGMENT

We would like to thank Universiti Teknikal Malaysia Melaka (UTeM), the Center for Research and Innovation Management (CRIM), and Centre for Telecommunication Research & Innovation (CeTRI) for their encouragement and motivation to conduct this research work.

REFERENCES

1. Jaiswal, A., S. Dey, M. P. Abegaonkar, and S. K. Koul, "Design and development of 60 GHz antenna integrated with RF MEMS SPDT switch for transceiver modules," *2018 IEEE International Symposium on Radio-frequency Integration Technology (RFIT)*, 1–3, IEEE, August 2018.
2. Algumaei, M. Y., N. A. Shairi, Z. Zakaria, A. M. S. Zobilah, and B. H. Ahmad, "Analysis of open stub resonator and its application in dual isolation band of SPDT switch design," *International Journal of Electrical and Computer Engineering*, Vol. 6, No. 6, 2900, 2016.
3. Hu, K. Z., M. C. Tang, Y. Wang, D. Li, and M. Li, "Compact, vertically integrated duplex filtenna with common feeding and radiating SIW cavities," *IEEE Transactions on Antennas and Propagation*, Vol. 69, No. 1, 502–507, 2020.
4. Hosain, M. M., S. Kumari, and A. K. Tiwary, "Compact filtenna for WLAN applications," *Journal of Microwaves, Optoelectronics and Electromagnetic Applications*, Vol. 18, 70–79, 2019.
5. Nasser, Z. A. A., Z. Zakaria, N. A. Shairi, S. N. Zabri, and A. M. Zobilah, "Design of compact filtenna based on capacitor loaded square ring resonator for wireless applications," *Progress In Electromagnetics Research M*, Vol. 96, 21–31, 2020.
6. Valizade, A., P. Rezaei, and A. A. Orouji, "A new design of dual-port active integrated antenna for 2.4/5.2 GHz WLAN applications," *Progress In Electromagnetics Research B*, Vol. 58, 83–94, 2014.
7. Bi, X., Q. Ma, C. Ning, and Q. Xu, "A compact switchable filtering diplexer based on reused L-shaped resonator," *IEEE Transactions on Circuits and Systems II: Express Briefs*, Vol. 65, No. 12, 1934–1938, 2018.
8. Li, Y. C., X. Fang, Q. Xue, and S. Chen, "Dual-mode filtering switches based on hybrid microstrip-cavity structures," *IEEE Transactions on Microwave Theory and Techniques*, Vol. 69, No. 8, 3853–3860, 2021.
9. Ma, K., Y. Wang, W. Li, and Y. Chen, "A novel compact self-packaged SPDT switchable BPFs based on SISL platform," *IEEE Transactions on Industrial Electronics*, Vol. 66, No. 9, 7239–7249, 2018.
10. Ma, K., S. Mou, and K. S. Yeo, "A miniaturized millimeter-wave standing-wave filtering switch with high P1 dB," *IEEE Transactions on Microwave Theory and Techniques*, Vol. 61, No. 4, 1505–1515, 2013.
11. Xu, J., Q. H. Cai, Z. Y. Chen, and Y. Q. Du, "Quasi-lumped-element filter-integrated single-pole double-throw switch," *IEEE Transactions on Microwave Theory and Techniques*, Vol. 65, No. 11, 4564–4571, 2017.
12. Zobilah, A. M., N. A. Shairi, Z. Zakaria, P. W. Wong, M. K. Zahari, M. Y. Q. Algumaei, and Z. A. A. Nasser, "Absorptive filter integrated single pole double throw switch using switchable T-shape resonator for IoT applications," *Progress In Electromagnetics Research C*, Vol. 103, 167–176, 2020.
13. Weng, S. C., K. W. Hsu, and W. H. Tu, "Microstrip bandpass single-pole quadruple-throw switch and independently switchable quadruplexer," *IET Microwaves, Antennas & Propagation*, Vol. 8, No. 4, 244–254, 2014.
14. Hou, F., Y. Shen, H. Luan, C. Sun, M. Huang, J. Zhu, and S. Hu, "Micropackaged compact switchable filters with high isolation in 3-D TSV-MEMS process," *IEEE Transactions on Components, Packaging and Manufacturing Technology*, Vol. 11, No. 4, 647–654, 2021.
15. Xu, J., F. Liu, Z. Y. Feng, and Y. F. Guo, "Diplexer-integrated spdt switches with multiple operating modes using common fractal stub-loaded resonator," *IEEE Transactions on Microwave Theory and Techniques*, Vol. 69, No. 2, 1464–1473, 2020.

16. Xu, J., H. Wan, and Z. Y. Chen, "Sharp skirt bandpass filter-integrated single-pole double-throw switch with absorptive OFF-state," *IEEE Transactions on Microwave Theory and Techniques*, Vol. 67, No. 2, 704–711, 2018.
17. Xu, J., F. Liu, and Z. Y. Feng, "Single-/dual-band bandpass filter-integrated single-pole double-throw switch using distributed coupling tri-mode resonators," *IEEE Transactions on Microwave Theory and Techniques*, Vol. 68, No. 2, 741–749, 2019.
18. Xu, J., Q. H. Cai, Y. F. Guo, S. Y. Ji, and Y. W. Duan, "A BPF integrated SP4T switch using parallel switched fractal common feeding line," *IEEE Transactions on Circuits and Systems II: Express Briefs*, Vol. 68, No. 6, 1932–1936, 2020.
19. Xu, J., Q. H. Cai, and Z. Y. Feng, "BPF-integrated SPDT switches with improved performance using frequency selective star-junction matching circuit and switched magnetic coupling technique," *IEEE Transactions on Microwave Theory and Techniques*, Vol. 68, No. 4, 1452–1461, 2019.
20. Xu, J. X., X. Y. Zhang, H. Y. Li, and Y. Yang, "Narrowband single-pole double-throw filtering switch based on dielectric resonator," *IEEE Microwave and Wireless Components Letters*, Vol. 28, No. 7, 594–596, 2018.
21. Pozar, D. M., *Microwave Engineering*, John Wiley & Sons, 2011.
22. Ibrahim, A. A., W. A. E. Ali, and M. A. Abdelghany, "Design of dual-band dual-mode bandpass filter utilizing 0° feed structure and lumped capacitors for WLAN/WiMAX applications," *Electronics*, Vol. 9, No. 10, 1697, 2020.
23. Hong, J. S. G. and M. J. Lancaster, *Microstrip Filters for RF/Microwave Applications*, John Wiley & Sons, 2004.
24. Chang, K. and L. H. Hsieh, *Microwave Ring Circuits and Related Structures*, Vol. 156, John Wiley & Sons, 2004.
25. Chaturvedi, S., S. V. Bhalke, G. Sai Saravanan, and S. K. Koul, "Electromagnetic simulation and characterization a metal ceramic package for packaging of high isolation switches," *Progress In Electromagnetics Research C*, Vol. 16, 111–125, 2010.
26. Hunter, I., *Theory and Design of Microwave Filters*, No. 48, 2001.
27. Xu, J., Q. H. Cai, and Z. Y. Chen, "A wideband bandpass filter integrated single-pole double-throw switch with wide stopband," *Frequenz*, Vol. 72, Nos. 11–12, 533–537, 2018.
28. Xu, J., Q. H. Cai, Z. Y. Chen, and Y. Q. Du, "Quasi-lumped-element filter-integrated single-pole double-throw switch," *IEEE Transactions on Microwave Theory and Techniques*, Vol. 65, No. 11, 4564–4571, 2017.